# Does the Threshold of Sediment Motion Constrain the Width of an Incising Laboratory River?

Thomas Christopher Ashley[1] and Kyle Strom[1]

[1]Virginia Tech

November 26, 2022

**Abstract**

A physically rational model for river width is critical to predict macroscopic landscape evolution driven by fluvial sediment transport. Growing evidence suggests that rivers widen until the stress exerted by the fluid on the bed surface is close to the critical entrainment stress of the bank material. In this study, we test the limits of this model as a closure assumption in dynamically evolving river systems. We consider a simple laboratory channel with a fixed water discharge, monodisperse bed material, no sediment supply, and an initial relief that was sufficiently large to guarantee a finite transport capacity. Over time, the transport capacity approaches zero through changes in channel morphology. Concurrent measurements of width and sediment load highlight departures from theory that mirror empirical trends in bankfull alluvial rivers. We suggest that lateral instability limits channel width at high sediment loads.

# Does the Threshold of Sediment Motion Constrain the Width of an Incising Laboratory River?

**T. C. Ashley[1], K. Strom[1]**

[1]Department of Civil & Environmental Engineering, Virginia Tech, Blacksburg, VA, USA

**Key Points:**

- Sediment discharge approaches zero in a laboratory river with no sediment supply.
- Width diverges from threshold prediction but follows empirical trends in alluvial rivers.
- Lateral instability appears to limit width when sediment discharge is high.

Corresponding author: T. C. Ashley, `tcashley@vt.edu`

## Abstract

A physically rational model for river width is critical to predict macroscopic landscape evolution driven by fluvial sediment transport. Growing evidence suggests that rivers widen until the stress exerted by the fluid on the bed surface is close to the critical entrainment stress of the bank material. In this study, we test the limits of this model as a closure assumption in dynamically evolving river systems. We consider a simple laboratory channel with a fixed water discharge, monodisperse bed material, no sediment supply, and an initial relief that was sufficiently large to guarantee a finite transport capacity. Over time, the transport capacity approaches zero through changes in channel morphology. Concurrent measurements of width and sediment load highlight departures from theory that mirror empirical trends in bankfull alluvial rivers. We suggest that lateral instability limits channel width at high sediment loads.



## Plain Language Summary

River channel width influences the rates and locations of large-scale geomorphic change. Recent studies argue that channel width is set by a balance between fluid and gravitational forces acting on sediment particles that make up the banks and bed. Here, we test whether this principle constrains the width of an incising laboratory river. Width remains roughly constant throughout the experiment, diverging from physical theory but mirroring observations of real rivers. To explain this behavior, we suggest that lateral instability prevents the formation of very wide, shallow river channels.


## 1 Introduction

Earth's surface is sculpted by water. In subaerial landscapes, water flows down topographic gradients and brings sediment on its journey from high to low elevations, reducing global relief over time. This process is usually unstable: feedbacks between flow, sediment transport, and topography amplify small perturbations and produce emergent, self-organized landforms like rivers, rills (Izumi & Parker, 2000; Loewenherz-Lawrence, 1994; Schorghofer et al., 2004), dunes, ripples, antidunes, and chevrons (Smith, 1970; Engelund & Fredsoe, 1982; Charru et al., 2013; Andreotti et al., 2012). The spontaneous formation of river channels is particularly important in the context of global geomorphic change because rivers enable transport of large volumes of material across low-gradient landscapes.

Climate, tectonics, and lithology provide the boundary conditions for fluvial processes. To model landscape evolution at this scale, rivers are typically represented as branching, one-dimensional conduits of water and sediment. Averaging over the recurrence interval of a formative, or "bankfull" flow condition (Wolman & Miller, 1960) introduces a logical separation between stochastic noise and macroscopic signals and allows a convenient simplification wherein each point on a river network (i.e., a "reach") is parameterized by characteristic values of state variables related to the flow, sediment load, channel geometry, bed composition, and fluxes across the channel boundary. Mathematical models for macroscopic river evolution may then be derived from conservative and constitutive relations between these state variables (Parker et al., 1998; Wickert & Schildgen, 2019). However, this effort has been hindered by a closure problem that is sometimes framed in terms of a missing equation for channel width (e.g., Parker, 1978; Paola et al., 1992; Parker et al., 1998; Dunne & Jerolmack, 2020; Phillips et al., 2022). Channel width is a key parameter for modeling reach-averaged sediment transport because it scales the fluid boundary stress associated with a given water discharge which, in turn, predicts the transport rate of different sediment sizes (e.g., Wilcock & Crowe, 2003; Wright & Parker, 2004). A physically-based model for channel width is therefore critical to understand the organization of fluvio-deltaic landscapes, predict and manage river response to human disturbance, and interpret past environmental conditions from the sedimentary record on Earth and Mars.

Over the last four decades, numerous studies have advanced the notion that river channels adjust their width $W$ so that the stress exerted by the fluid on the bed surface at the bankfull flow condition $\tau$ is close to the critical stress needed to mobilize the material that makes up the banks and bed, $\tau_c$ (Phillips et al., 2022, references therein). This basic reasoning is encapsulated by the "$1 + \varepsilon$" model, i.e.,:

$$\tau = (1 + \varepsilon)\tau_c \tag{1}$$

where $\varepsilon \ll 1$. Despite its broad appeal, this model lacked rigorous theoretical justification until recently due to the inherent difficulty of modeling hydraulics and sediment transport over arbitrarily sloping beds (e.g., Seminara et al., 2002; Parker et al., 2003). Popović et al. (2021) present a comprehensive analysis of this problem that ultimately supports the $1+\varepsilon$ hypothesis. Although the detailed derivation and testing depends on the assumption that flow is laminar, the underlying physical reasoning is also thought to be valid for turbulent flows. Critically, their model describes a stable configuration where width is constant, there are no overbank fluxes, and the sediment load $Q_s$ is spatially uniform ($dQ_s/dx = 0$).

What remains unclear is how channels achieve this stable state following a perturbation. This is problematic because rivers are continuously responding to climatic, tectonic, autogenic, and anthropogenic perturbations over a wide range of scales. Indeed, finite sediment loads are essentially an outcome of perturbation; the sediment load in any given reach integrates longitudinal gradients in transport rate over the contributing drainage area, precluding globally-uniform transport conditions. Tight empirical scaling relationships suggests that rivers can quickly adjust their width in response to perturbations (Phillips et al., 2022), and it may be reasonable to neglect small longitudinal gradients in sediment load for the purpose of predicting channel width in some cases. However, rapidly aggrading (Kim & Jerolmack, 2008) and incising (Croissant et al., 2017) channels exhibit dynamic changes in width that are not predicted by (1) but directly influence locations and rates of geomorphic change. This observation prompts several questions. First, what sets the relative timescales of adjustment of reach-averaged parameters like width and sediment supply? Second, what are the limits of the $1 + \varepsilon$ model as a closure assumption in macroscopic morphodynamic models? In other words, is the modeling framework presented by Phillips et al. (2022) appropriate for predicting the the width of aggrading and incising channels?

Presently, we investigate these questions using a simple laboratory experiment. Our objective was to create an incising alluvial channel ($dQ_s/dx > 0$) and document the transient process of adjustment towards the stable state ($dQ_s/dx = 0$). To this end, we carved a straight channel in uniform cohesionless substrate and imposed a constant water discharge. The initial relief was sufficiently large to guarantee a finite transport capacity but no sediment was supplied at the inlet. Because water discharge and grain size are fixed, the system achieves a stable state through morphological changes that reduce the sediment transport capacity. Concurrent measurements of sediment discharge and width provide a direct test of the $1 + \varepsilon$ model as described in the next section.

## 2 Theory

The concept of channel "stability" implies morphological invariance through time. Per the Exner equation (Paola & Voller, 2005), topography is stable when divergence of the sediment flux is constant everywhere, i.e.:

$$\frac{\partial q_{s,x}}{\partial x} + \frac{\partial q_{s,y}}{\partial y} = -(1 - p)\Psi. \tag{2}$$

Here, $q_{s,x}$ is the longitudinal component of the flux, $q_{s,y}$ is the lateral component of the flux, $p$ is the bed porosity and $\Psi$ is a rate of bed elevation change with respect to a datum that tracks uplift and subsidence. To predict channel width from physical theory, researchers seek solutions to (2) that incorporate simplified models for hydraulics and sediment transport. Recognizing that all rivers exhibit stochastic fluctuations in reach-averaged state variables like width, it is often implicitly assumed that such solutions describe a deterministic expectation associated with a probabilistic ensemble of possible channel geometries conditional on appropriately defined boundary conditions.

The "threshold" channel is a trivial solution to this problem where $q_{s,x} = q_{s,y} = 0$. It follows that channel geometry balances fluid, friction, and gravitational forces acting on particles resting on the bed surface. Neglecting lateral diffusion of fluid momentum and assuming (a) the water discharge discharge $Q_w$ is fixed, (b) the bed material is uniform and cohesionless with a representative diameter $D$ and (c) all of the flow resistance comes from grains, granular forces are balanced across the entire channel if the cross-sectional shape $h(y)$ follows a cosine function with a constant aspect ratio of $W/H = \pi^2/(2\mu) \approx 7$, where $W$ is the width, $H$ is the mean flow depth, and $\mu \approx 0.7$ is the critical friction angle of the bed material, that is (Glover & Florey, 1951; Savenije, 2003; Devauchelle et al., 2011; Seizilles et al., 2013):

$$h(y) = \frac{\pi}{2} H \cos\left(\frac{\pi y}{W}\right) \tag{3}$$

To accommodate a specified water discharge, width and slope $S$ must satisfy

$$W_0 = D \frac{\pi}{\alpha\sqrt{\mu}} \frac{\sqrt{C_f Q_{w*}}}{\tau_{*c}^{1/4}} \tag{4}$$

and

$$S_0 = \frac{\alpha}{\sqrt{\mu}} \frac{R\tau_{*c}^{5/4}}{\sqrt{C_f Q_{w*}}}. \tag{5}$$

Here, the subscript 0 denotes values of $W$ and $S$ predicted for the threshold channel, $Q_{w*} = Q_w/\sqrt{gRD^5}$ is a dimensionless water discharge, $\tau_{*c} = \tau_c/\rho gRD$ is a dimensionless critical stress for sediment motion, $C_f = \sqrt{gHS}/U$ is a flow resistance factor, $U$ is the mean flow velocity, $R$ is the submerged specific gravity of the sediment, $g$ is gravitational acceleration, and $\alpha = (8/\pi)^{1/4}$. While the precise value of $\alpha$ depends on the flow model, defensible choices evaluate to $\alpha = O(1)$. Throughout this paper, we assume fixed values of $C_f = 0.1$, $R = 1.66$, $g = 9.81 \mathrm{m/s}^2$, and $\tau_{*c} = 0.04$ such that $W_0$ and $S_0$ depend only on $Q_w$ and $D$.

The threshold solution was recently extended to include laminar channels with finite sediment loads assuming that the sediment load is constant in the longitudinal direction ($dQ_s/dx = 0$) (Popović et al., 2021). This implies that $\Psi = 0$ and $q_{s,y} = 0$ on the channel margins (i.e. there is no erosion or aggradation and no overbank fluxes) and allows (2) to be expressed as an ordinary differential equation that can be solved numerically. In this case, diffusive fluxes of sediment and fluid momentum exert first-order control on the dimensionless excess stress $\varepsilon = \tau/\tau_c - 1$ which, in turn, scales the width averaged sediment flux $q_s = Q_s/W$ per an appropriate sediment transport formula (e.g., Wong & Parker, 2006). Mathematical, numerical, and experimental tests reveal two distinct scaling regimes that are delineated by $Q_s$. At low $Q_s$, width is effectively constant and changes in sediment supply are accommodated through changes in $\varepsilon$. At high $Q_s$, $\varepsilon$ and $q_s$ saturate at fixed values $\varepsilon_0$ and $q_{s0}$, and changes in sediment supply are accommodated through changes in width. Popović et al. (2021) find that $\varepsilon_0 \approx 0.2$, supporting the hypothesis that rivers cannot maintain large excess stresses (i.e., $\varepsilon \ll 1$ as proposed by Parker, 1978). We propose the following expression to approximates this behavior over the full range of sediment loads:

$$\frac{W}{W_0} = (1 + Q_{s*}^k)^{1/k}. \tag{6}$$

Here $Q_{s*} = Q_s/[q_{s0}W_0]$ and $k$ is a parameter that scales the smoothness of the transition between regimes at $Q_{s*} = 1$. We find that $k = 5$ provides a reasonable fit to data presented by Abramian et al. (2020). This expression is identical to the $1+\varepsilon$ model except at very low transport rates ($Q_{s*} < 1$). We emphasize that the laminar flow assumption simplifies their mathematical derivation; however, the underlying physical reasoning is generally thought to be valid for turbulent flows.

The relationship between width and slope can be predicted by substituting a sediment transport formula into (6). In effect, the result is identical to the $1+\varepsilon$ model except when $S \approx S_0$. Neglecting nonlinearity close to $S_0$ leads to (Dunne & Jerolmack, 2020):

$$\frac{W}{W_0} = \frac{1}{(1+\varepsilon_0)^{3/2}} \frac{S}{S_0} \tag{7}$$

In other words, excess width is expected to increase in proportion to excess slope.

In summary, Popović et al. (2021) show that the $1 + \varepsilon$ model constrains the relationship between $W$ and $Q_s$ when $dQ_s/dx = 0$ up to the point where lateral instability produces braiding. A key question is whether this relationship remains valid when $dQ_s/dx \neq 0$. This question is crucial because longitudinal gradients in transport rate are explicitly tied to macroscopic landscape evolution. Below, we present a direct empirical test of equation (6) using concurrent measurements of $Q$ and $W$ in an incising laboratory channel. Then, we reinterpret empirical trends in a global database of alluvial rivers (Dunne & Jerolmack, 2018) in light of our experimental results and equation (7).

## 3 Experiment

### 3.1 Setup

The experiment was conducted in a 1.2 m wide by 2.9 m long rectangular stream table elevated over a standing basin of water (Figure 1c). A wire mesh enclosure was placed at the upstream end and filled with gravel ($D_{50} \approx 2$ cm) to dissipate fluid energy. This enclosure spanned the entire width of the stream table, allowing the channel to self-select its inlet width. The stream table was then filled with 0.3 m$^3$ of sand with a measured density of $\rho_s = 2.66$ g/cm$^3$, median diameter of $D_{50}$ =0.4 mm, and base-2 logarithmic standard deviation of $\sigma_\phi = 0.72$. The sand was leveled to a constant thickness of 12 cm except at the downstream end where the bed surface sloped downward towards the edge of the stream table. Then, a straight, triangular channel with banks at the angle of repose was carved down the center of the experimental domain.

Water was pumped from the standing basin into a head tank, supplying a constant discharge of 0.16 L/s. Given these conditions and assumed values of fixed parameters, equation (4) predicts $W_0 = 9.1$ cm. After filling the gravel enclosure, water flowed through the channel to the outlet and spilled over the edge of the metal platform into the standing basin. In effect, this setup fixes the base level position throughout the duration of the experiment. Time $t$ is measured from the instant that the water reached the downstream end of the experimental domain.

Lateral channel migration was unrestricted at the downstream end except by the sides of the stream table. The channel briefly touches one side but never touches both sides simultaneously; we argue that width was never restricted by the dimensions of the streamtable. Water discharge measured at the inlet and outlet differed by less than 5%, indicating that groundwater flow was negligible. Overhead photos and topography scans were collected throughout the experiment to quantify changes in channel width and sediment discharge. The overhead images were also used to ensure the water surface position in the head tank remained constant. The experiment was ended when there were

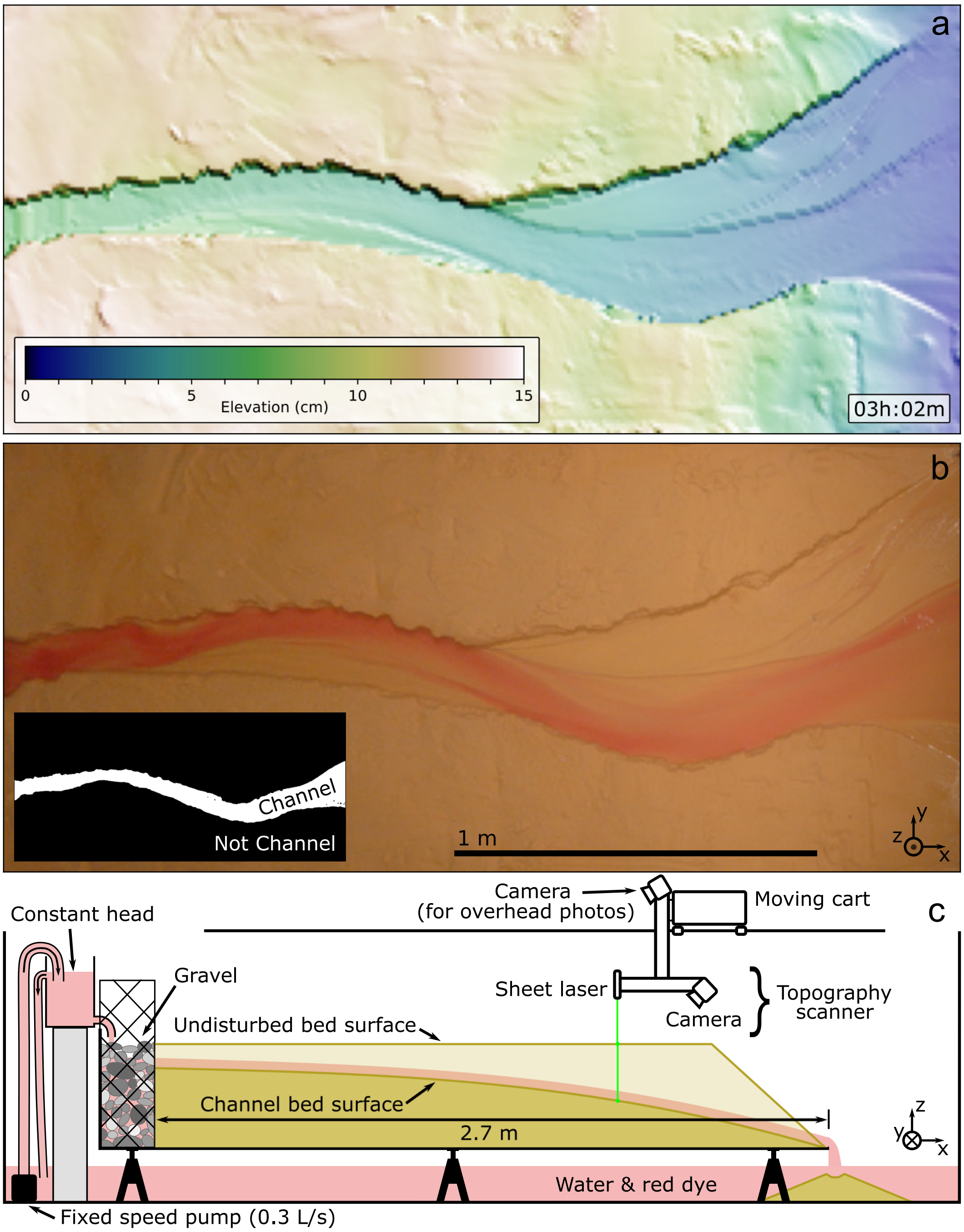


**Figure 1.** Experimental data and setup (a) an example elevation model after processing, (b) an example orthorectified overhead photo and the output of our automated channel identification algorithm (inset). (c) a schematic highlighting elements of the experimental setup.

no observable changes in overhead photos over a period of 24 hours. This took approximately 340 hours (14 days).

Below, we provide a brief overview of the data acquisition and analysis methods used in this study. Detailed processing workflows and a video of the experiment are available with the published dataset (Ashley & Strom, 2022).

### 3.2 Measurements of Sediment Discharge

Sediment discharge is calculated from repeat scans of topography (Figure 1a) obtained using a SICK Ranger E50 3-D laser scanning system mounted to a moving cart (see also: Hoyal & Sheets, 2009; Hamilton et al., 2015). The scan interval was increased from 30 minutes to 8 hours throughout the experiment. Each scan comprises 9 overlapping passes with the laser system, producing between 3 and 9 measurements of bed elevation for every 1 mm $\times$ 1 mm region of the bed. Measurements were merged using a custom algorithm to obtain final elevation models at 1 cm resolution.

The average sediment discharge $\overline{Q_s}(x, t_0, t_1)$ past the longitudinal position $x$ between two topography scans obtained at $t_0$ and $t_1$ is estimated by dividing the change in sediment volume upstream of $x$ by the time between scans, $t_1 - t_0$. A detailed derivatin of this expression is presented by Ashley and Strom (2022). Throughout the remainder of this paper, we interpret the average sediment discharge $\overline{Q_s}(x, t_0, t_1)$ as a proxy for the instantaneous ensemble average at $t = \sqrt{t_0 t_1}$, the geometric midpoint of $t_0$ and $t_1$. In total, we report 676 measurements of sediment discharge corresponding to 26 different times and 26 different longitudinal positions.

### 3.3 Measurements of Channel Width

Channel width was estimated from overhead photos (Figure 1b) collected at an interval that increased from 1 to 16 minutes throughout the experiment. No images were acquired from approximately $t = 17.2$ to $t = 23.2$ hours due to a camera malfunction. Images were also not acquired for approximately six minutes during each topography scan.

An automated channel identification algorithm was used to extract 2680 width measurements (at 1 mm longitudinal resolution) each from 3498 images. The main element of this algorithm is a logistic regression model (fit using three manually digitized channel masks) that predicts the probability that each pixel is part of the channel as a function of lightness-corrected red, green, and blue bands. Probabilities are predicted for each pixel, smoothed in space, and thresholded at $p = 0.5$. Finally, width is calculated by summing the total number of channel pixels at each longitudinal position and multiplying by the pixel width. This approach correctly differentiates between wet and dry pixels with 97% accuracy in the training dataset. 68% of the predicted widths lie within a factor of 1.2 of the measured width, and all widths lie within a factor of 1.9 of the measured width. The algorithm was spot-checked to ensure results are reasonable outside the training dataset. Finally, average widths are computed at a spatiotemporal resolution that matches the 676 reported sediment discharge measurements to enable a direct comparison of these quantities.

## 4 Phases of Adjustment

The data described above document transient river adjustment at an unprecedented level of detail. In this section, we integrate data and observations to identify key processes associated with morphologically-mediated relaxation towards the threshold state. Our goal is to establish a phenomenological context for the comparison of data and theory presented in Section 5.

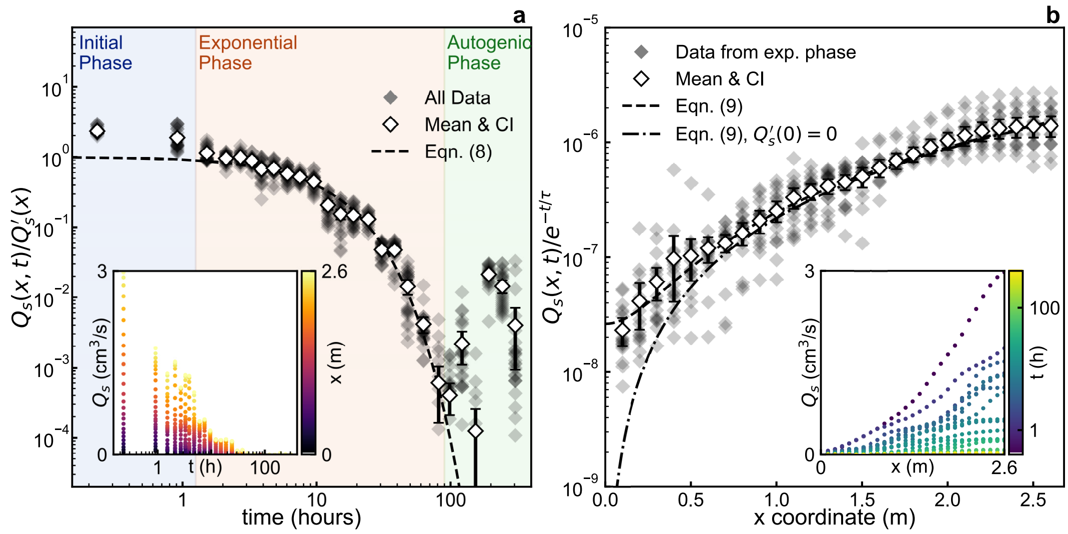


**Figure 2.** Spatial and temporal evolution of the sediment discharge. Panels (a) and (b) show collapsed raw data (insets) to highlight the predominant trend described by equations (8) and (9). Only data from the exponential phase are plotted in panel (b). Means and 95% confidence intervals (CI) are computed from collapsed data.

Measurements of sediment discharge (Figure 2, insets) and qualitative changes in channel behavior observed in timelapse images (Ashley & Strom, 2022) indicate that morphological evolution is fastest at the beginning of the experiment and then slows over time. We identify three distinct intervals, referred to throughout the remainder of this paper as "initial", "exponential" and "autogenic" phases of adjustment. Most (75%) of the morphological change occurs during the exponential phase which begins at $t \approx 1.25$ hours and ends at $t \approx 90$ hours. This phase is characterized by a highly regular pattern of spatial and temporal variability in the average sediment discharge, while the initial and autogenic phases are characterized by deviations from this pattern (Figure 2). Approximately 15% of the total geomorphic change occurs during the initial phase and 10% occurs during the autogenic phase.

During the exponential phase, the sediment discharge $Q_s(x,t)$ at each cross-section (i.e., each $x$) decreases exponentially over time (Figure 2a, Exponential Phase), i.e., is well described by:

$$Q_s(x,t) = Q_s'(x)e^{-t/T_c}. \tag{8}$$

Here, $Q_s'(x)$ is a parameter that is analogous to an initial sediment discharge at $x$ (see below) and $T_c$ is a characteristic exponential timescale. A single value of $T_c = 11$ hours provides a good fit for every $x$, and the longitudinal profile of the sediment load maintains a constant shape, varying in uniform proportion to $Q_s'(x)$. The following expression constrains this shape (Figure 2b):

$$\frac{Q_s'(x)}{Q_s'(L)} = \frac{Q_s'(0)}{Q_s'(L)} + \left(\frac{x}{L}\right)^2. \tag{9}$$

Here, $L$ is the length of the experimental domain. Thus, the sediment discharge at any $x$ and $t$ can be predicted from four parameters: $Q_s'(0)$, $Q_s'(L)$, $T_c$, and $L$. Note that the a finite best-fit value of $Q_s'(0)$ reflects a boundary effect characterized by enhanced bank erosion where flow accelerates at the inlet. This effect is visible as an incipient triangular wedge on the left side of Figure 1. Because the boundary effect is relatively small, assuming $Q_s'(0) = 0$ provides a good fit except near the upstream boundary (Figure 2b).

Prior to $t = 1.25$ hours, measured sediment discharges are significantly higher than predicted from the best-fit exponential function (Figure 2a, Initial Phase). Consequently, $Q'_s(x)$ is not the true sediment discharge at $t = 0$; rather, it is a parameter that scales the sediment discharge during the exponential phase.

We suggest that the spatially-uniform exponential timescale is indicative of a quasi-stable condition where local state variables are dictated entirely by the global configuration of the system. In other words, the parameters $Q'_s(L)$, and $T_c$ are governed by global boundary conditions like $Q_w$, $D$, $L$, and the initial relief. Recognizing that the initial channel was straight and had a triangular shape with banks close to the angle of repose, we believe the enhanced transport during the initial phase reflects rapid morphological changes that lead to this quasi-stable configuration. This conclusion is supported by rapid changes in width in the first 20 minutes of the experiment (Figure 3) and increases in sinuosity observed in timelapse images.

Although spatially uniform exponential relaxation is not predicted by existing physical theory, we note that the the total average longitudinal flux $Q_s/1.2$ m, (i.e. averaging over the width of the experimental domain including the channel and floodplain) follows a solution for one-dimensional landscape evolution driven by linear diffusion. Our simple fluvial landscape exhibits rich similarity to diffusion-dominated landscapes like hillslopes, supporting a hypothesis proposed by Reitz et al. (2014).

Significant departures from exponential relaxation are observed after $t = 90$ hours. During this time, autogenic pulses of incision are separated by periods of relative stasis. Broadly, we believe this behavior is an outcome of nonlinearity in transport rate as a function of shear stress close to the threshold of sediment motion. Departures may also reflect a failure of the assumption that short temporal averages are a good proxy for ensemble averages. The overall effect is that intermittent transport processes appear to persist for much longer than expected given the exponential trend observed during the previous phase.

## 5 Channel Width

### 5.1 First Order Trend

Our simplified approximation of the model presented by Popović et al. (2021) (Equation 6), predicts that widths should increase in proportion to $Q_s$ when $Q_s > q_{s0}W_0$. Throughout the experiment, measurements of $Q_s$ vary by a factor of $O(10^5)$, leading to predicted widths that are as large as $O(10^2)\times W_0$. However, measured widths remain within a factor of $O(10^1)$ of the threshold width throughout the experiment (Figure 3a). We emphasize that this result is incompatible with the $1 + \varepsilon$ model and the model of Popović et al. (2021). Most importantly, widths do not increase with $Q_{s*}$ as expected when $Q_{s*} > 1$ as shown in figure 3b.

Although our results are not compatible with the $1+\varepsilon$ model, they are consistent with first-order empirical trends in bankfull alluvial rivers (Figure 3c). Dunne and Jerolmack (2018) show that rivers remain close to $W_0$ across a wide range of conditions and settings, even when they are significantly steeper than the $S_0$. Additionally, the range of $W/W_0$ values observed in our experiment is comparable to the range of values observed in bankfull alluvial rivers on Earth's surface.

This result is significant because hydraulic considerations require

$$\frac{\tau}{\tau_c} = \left[\frac{S}{S_0}\frac{W_0}{W}\right]^{2/3}. \tag{10}$$

Thus, if $W \approx W_0$ and $S \gg S_0$, then $\tau \gg \tau_c$. This relationship is highlighted by isocontours of constant $\tau/\tau_c$ in Figure 3c. The same isocontours are plotted in Figure 3b

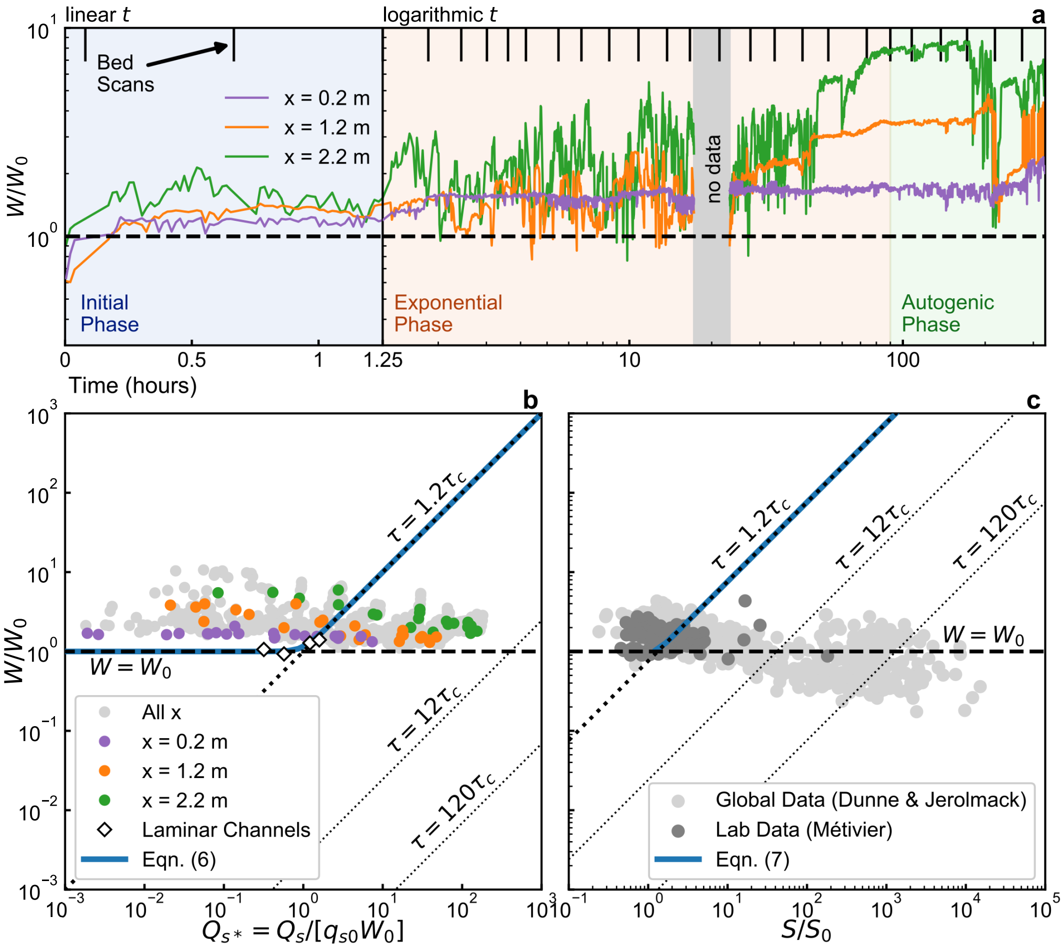


**Figure 3.** Width measurements compared with theory and other data. Although the magnitude of width fluctuations varies in space and time, the central tendency remains close to $W_0$, mirroring empirical trends in field and laboratory data. (a) High resolution measurements of width at three representative cross section. (b) Comparison of average widths and sediment discharges with (6). Note that $q_{s0}$ is the sediment flux corresponding to $\varepsilon = 0.2$ and is computed after Wong and Parker (2006) for our experiment. This is appropriate because flow is turbulent and inferred stresses cannot suspend bed material. (c) Comparison of field (Dunne & Jerolmack, 2018) and laboratory (Métivier et al., 2017) data with equation (7).

assuming $q_s = f(\tau)$ per Wong and Parker (2006). Note that these isocontours are plotted for illustrative purposes; our primary result is not sensitive to the choice of bedload transport formula used here.

Several mechanisms have been proposed to explain this observation including enhanced bank strength (e.g., Dunne & Jerolmack, 2018, references therein) and stress partitioning (Francalanci et al., 2020). While these are sufficient to explain elevated stresses with respect to $\tau_c$, they are not predictive because they introduce additional model parameters that preclude mathematical closure (for example, the critical stress of the bank material). Our experiments reproduce trends observed in stable laboratory channels and bankfull alluvial rivers using cohesionless, uniform bed material, evincing a fundamental organizing principle that (a) does not rely on enhanced bank strength and (b) is valid even when $dQ_s/dx \neq 0$.

### 5.2 Instability-Limited Width

High resolution measurements of width (Figure 3a) reveal deviations from the first-order trend described above. Width fluctuates rapidly, and though the magnitude of fluctuations increases in the downstream direction, every cross-section periodically returns to $W_0$. In plan view, fluctuations are reminiscent of periodic oscillations between channelized transport and sheet flow described in an aggrading fan delta by Kim and Jerolmack (2008). These authors document coupled changes in width and slope that are linked to autogenic pulses of proximal and distal deposition and argue that periods of narrowing are initiated by a lateral instability mechanism that is analogous to the channelization instability on hillslopes (Izumi & Parker, 2000; Loewenherz-Lawrence, 1994; Schorghofer et al., 2004).

We hypothesize that a similar mechanism sets the upper limit of width fluctuations in our experiment. When $W \approx W_0$, the channel tends to widen, perhaps through the classically-envisioned mechanism associated with bedload transport on laterally sloping banks (e.g., Parker, 1978). However, as the total width of the channel increases, depth decreases and the channel becomes laterally unstable due to small variations in shear stress and sediment flux. Eventually, runaway incision in a small part of the wetted perimeter causes narrowing that stops as $W$ approaches $W_0$. This lower limit may be set by the angle of repose of the bed material; widths below $W_0$ require very steep banks that are susceptible to gravitational failure.

Because similar processes have been described in aggrading subaerial (Kim & Jerolmack, 2008) and submarine (Hamilton et al., 2013) fan deltas, we suggest that the channelization instability sets an important upper limit on channel width regardless of the sign and magnitude of the longitudinal gradient in transport rate. We further hypothesize that periodic widening and narrowing is connected to lateral sediment motion that looks like diffusion averaged over a characteristic timescale of width fluctuations. Consequently, the average width might be modeled in a framework similar to Popović et al. (2021) by adopting an appropriate model for morphodynamically-enhanced lateral sediment diffusion.

Previous authors have recognized the importance of lateral instability at high slopes (Reitz et al., 2014; Abramian et al., 2020; Popović et al., 2021) and argue that braiding partitions water into smaller threads that are each threshold channels (i.e. $W = W_0$ and $\tau = (1+\varepsilon)\tau_c$). In this case, the total width of all threads is predicted to scale with $Q_*$ and $S/S_0$ per (6) and (7). Our hypothesis differs from these studies in that we suggest lateral instability actually limits increases in width above roughly $10W_0$.

This dynamic process of widening and narrowing only occurs in two of the three representative cross-sections highlighted in figure 3a. In the cross-section located at $x =$ 0.2 m, width is almost invariant after the initial phase of adjustment. We hypothesize that rapid fluctuations in width are absent because the stable width corresponding to $\tau \approx \tau_c$ is less than a critical width where the channel becomes susceptible to instability. In other words, the channel is able to achieve a true stable configuration as envisioned by (Popović et al., 2021) when the sediment load is small.

## 6 Summary and Implications

Our experiment highlights dynamic fluctuations in channel width and sediment discharge throughout the process of incisional relaxation toward the threshold state. After an initial period of rapid adjustment, the sediment discharge decays over a spatially uniform exponential timescale. At long timescales, this pattern breaks down and sediment transport occurs primarily through intermittent, autogenic events.

Our primary finding is that width remains close to the width of the threshold channel across a wide range of sediment loads. As a result, changes in sediment supply are accommodated primarily through changes in the unit sediment discharge rather than changes in width. This result is surprising because it diverges from established physical theory (e.g., Popović et al., 2021), however; it mirrors empirical trends in bankfull alluvial rivers. Previously, large excess stresses needed to produce large fluxes have been attributed to differences between the critical stress of the bank material and the critical stress of the bed material (Dunne & Jerolmack, 2018, 2020), but our experiment reproduces this trend using cohesionless, uniform bed material.

To explain our observations, we argue that two distinct mechanisms can limit channel width. When sediment load is small, channel geometry balances lateral advective and diffusive sediment fluxes and the width is “threshold-limited” (Dunne & Jerolmack, 2018, 2020; Phillips et al., 2022). At higher sediment loads, the channel cannot achieve a stable configuration because the shape that balances lateral fluxes is susceptible to internal channelization. In this case, the average width is “instability-limited”. The hypothesized transition from threshold-limitation to instability-limitation explains why Abramian et al. (2020) observed small increases in width associated with changes in sediment supply, but no combination of reach-scale boundary conditions can produce stable widths that are significantly larger than $O(10^1)\times W_0$. It also provides a physically rational explanation for empirical trends in alluvial rivers (Figure 3c) and leads to a first-order prediction of bed stress (Per equation 10) that does not depend on an extra parameter like the critical stress of the bank material.

**Acknowledgments**
We thank Doug Jerolmack for many fruitful discussions. We also thank Kerry Desmond for valuable assistance running experiments. Data and workflows are available on GitHub (Ashley & Strom, 2022).

## References

Abramian, A., Devauchelle, O., & Lajeunesse, E. (2020). Laboratory rivers adjust their shape to sediment transport. *Physical Review E*, *102*(5), 1–10. doi: 10.1103/physreve.102.053101

Andreotti, B., Claudin, P., Devauchelle, O., Durán, O., & Fourrière, A. (2012). Bedforms in a turbulent stream: Ripples, chevrons and antidunes. *Journal of Fluid Mechanics*, *690*, 94–128. doi: 10.1017/jfm.2011.386

Ashley, T. C., & Strom, K. (2022). *Relaxing channel data and workflows.* Github Repository. doi: 10.5281/zenodo.6573440

Charru, F., Andreotti, B., & Claudin, P. (2013). Sand ripples and dunes. *Annual Review of Fluid Mechanics*, *45*(1), 469–493. doi: 10.1146/annurev-fluid-011212-140806

Croissant, T., Lague, D., Steer, P., & Davy, P. (2017). Rapid post-seismic landslide evacuation boosted by dynamic river width. *Nature Geoscience*, *10*(9), 680–684. doi: 10.1038/ngeo3005

Devauchelle, O., Petroff, A. P., Lobkovsky, A. E., & Rothman, D. H. (2011). Longitudinal profile of channels cut by springs. *Journal of Fluid Mechanics*, *667*, 38–47. doi: 10.1017/S0022112010005264

Dunne, K. B., & Jerolmack, D. J. (2018). Evidence of, and a proposed explanation for, bimodal transport states in alluvial rivers. *Earth Surface Dynamics*, *6*, 583–594. doi: 10.5194/esurf-6-583-2018

Dunne, K. B., & Jerolmack, D. J. (2020). What sets river width? *Science Advances*, *6*(41), 1–9. doi: 10.1126/sciadv.abc1505

Engelund, F., & Fredsoe, J. (1982). Sediment ripples and dunes. *Annual Review of Fluid Mechanics*, *14*(1), 13–37. doi: 10.1146/annurev.fl.14.010182.000305

Francalanci, S., Lanzoni, S., Solari, L., & Papanicolaou, A. N. (2020). Equilibrium Cross Section of River Channels With Cohesive Erodible Banks. *Journal of Geophysical Research: Earth Surface*, *125*(1), 1–20. doi: 10.1029/2019JF005286

Glover, R. E., & Florey, Q. L. (1951). Stable channel profiles. *US Department of the Interior Hydraulic Laboratory Report*, *Hyd-235*.

Hamilton, P. B., Strom, K., & Hoyal, D. C. (2013). Autogenic incision-backfilling cycles and lobe formation during the growth of alluvial fans with supercritical distributaries. *Sedimentology*, *60*(6), 1498–1525. doi: 10.1111/sed.12046

Hamilton, P. B., Strom, K. B., & Hoyal, D. C. (2015). Hydraulic and sediment transport properties of autogenic avulsion cycles on submarine fans with supercritical distributaries. *Journal of Geophysical Research F: Earth Surface*, *120*(7), 1369–1389. doi: 10.1002/2014JF003414

Hoyal, D. C., & Sheets, B. A. (2009). Morphodynamic evolution of experimental cohesive deltas. *Journal of Geophysical Research: Earth Surface*, *114*(2), 1–18. doi: 10.1029/2007JF000882

Izumi, N., & Parker, G. (2000). Linear stability analysis of channel inception: Downstream-driven theory. *Journal of Fluid Mechanics*, *419*, 239–262. doi: 10.1017/S0022112000001427

Kim, W., & Jerolmack, D. J. (2008). The pulse of calm fan deltas. *Journal of Geology*, *116*(4), 315–330. doi: 10.1086/588830

Loewenherz-Lawrence, D. S. (1994). Hydrodynamic description for advective sediment transport processes and rill initiation. *Water Resources Research*, *30*(11), 3203–3212. doi: 10.1029/94WR02076

Métivier, F., Lajeunesse, E., & Devauchelle, O. (2017). Laboratory rivers: Lacey's law, threshold theory, and channel stability. *Earth Surface Dynamics*, *5*, 187–198. doi: 10.5194/esurf-5-187-2017

Paola, C., Heller, P., & Angevine, C. (1992). The large-scale dynamics of grain-size variation in alluvial basins, 1: Theory. *Basin Research*, *4*, 73–90.

Paola, C., & Voller, V. R. (2005). A generalized Exner equation for sediment mass balance. *Journal of Geophysical Research: Earth Surface*, *110*(4), 1–8. doi: 10.1029/2004JF000274

Parker, G. (1978). Self-formed straight rivers with equilibrium banks and mobile bed. Part 2. The gravel river. *Journal of Fluid Mechanics*, *89*, 127–146. doi: 10.1017/S0022112078002505

Parker, G., Paola, C., Whipple, K. X., & Mohrig, D. (1998). Alluvial fans formed by channelized fluvial and sheet flow. I: theory. *Journal of Hydraulic Engineering*, *124*(10), 985–995. doi: 10.1061/(ASCE)0733-9429(1998)124:10(985)

Parker, G., Seminara, G., & Solari, L. (2003). Bed load at low Shields stress on arbitrarily sloping beds: Alternative entrainment formulation. *Water Resources Research*, *39*(7), 1–11. doi: 10.1029/2001WR001253

Phillips, C. B., Francalanci, S., Lanzoni, S., Merritts, D. J., Lajeunesse, E., &

Jerolmack, D. J. (2022). Threshold constraints on the size, shape and stability of alluvial rivers. *Nature Reviews Earth & Environment*. doi: 10.1038/s43017-022-00282-z

Popović, P., Devauchelle, O., Abramian, A., & Lajeunesse, E. (2021). Sediment load determines the shape of rivers. *Proceedings of the National Academy of Sciences*, *118*(49). doi: 10.1073/pnas.2111215118

Reitz, M. D., Jerolmack, D. J., Lajeunesse, E., Limare, A., Devauchelle, O., & Métivier, F. (2014). Diffusive evolution of experimental braided rivers. *Physical Review E - Statistical, Nonlinear, and Soft Matter Physics*, *89*, 1–6. doi: 10.1103/PhysRevE.89.052809

Savenije, H. H. (2003). The width of a bankfull channel; Lacey's formula explained. *Journal of Hydrology*, *276*, 176–183. doi: 10.1016/S0022-1694(03)00069-6

Schorghofer, N., Jensen, B., Kudrolli, A., & Rothman, D. H. (2004). Spontaneous channelization in permeable ground: Theory, experiment, and observation. *Journal of Fluid Mechanics*, *503*, 357–374. doi: 10.1017/S0022112004007931

Seizilles, G., Devauchelle, O., Lajeunesse, E., & Metivier, F. (2013). Width of laminar laboratory rivers. *Physical Review E - Statistical, Nonlinear, and Soft Matter Physics*, *87*, 1–5. doi: 10.1103/PhysRevE.87.052204

Seminara, G., Solari, L., & Parker, G. (2002). Bed load at low Shields stress on arbitrarily sloping beds: Failure of the Bagnold hypothesis. *Water Resources Research*, *38*(11). doi: doi:10.1029/2001WR000681

Smith, J. D. (1970). Stability of a sand bed subjected to a shear flow of low Froude number. *Journal of Geophysical Research*, *75*(30), 5928. doi: 10.1029/JC075i030p05928

Wickert, A. D., & Schildgen, T. F. (2019). Long-profile evolution of transport-liomited gravel-bed rivers. *Earth Surface Dynamics*, *7*, 17–43. doi: https://doi.org/10.5194/esurf-7-17-2019

Wilcock, P. R., & Crowe, J. C. (2003). Surface-based transport model for mixed-size sediment. *Journal Hydraulic Engineering*, *129*(2), 120–128. doi: 10.1061/(ASCE)0733-9429(2003)129:2(120)

Wolman, M. G., & Miller, J. P. (1960). Magnitude and frequency of forces in geomorphic processes. *The Journal of Geology*, *68*(1), 54–74. doi: 10.1086/626637

Wong, M., & Parker, G. (2006). Reanalysis and correction of bed-load relation of Meyer-Peter and Müller using their own database. *Journal of Hydraulic Engineering*, *132*(11), 1159–1168. doi: 10.1061/(ASCE)0733-9429(2006)132:11(1159)

Wright, S. A., & Parker, G. (2004). Flow resistance and suspended load in sand-bed rivers: Simplified stratification model. *Journal of Hydraulic Engineering*, *130*(8), 796–805. doi: 10.1061/(ASCE)0733-9429(2004)130:8(796)